# Multi-modal Registration Improves Group Discrimination in Pediatric Traumatic Brain Injury

Emily L. Dennis[1], Faisal Rashid[1], Julio Villalon-Reina[1], Gautam Prasad[1], Joshua Faskowitz[1], Talin Babikian[2], Richard Mink[3], Christopher Babbitt[4], Jeffrey Johnson[5], Christopher C. Giza[6], Robert F. Asarnow[2,7,8], Paul M. Thompson[1,2,9]

[1]Imaging Genetics Center, Keck USC School of Medicine, Marina del Rey, CA, USA; [2]Department of Psychiatry and Biobehavioral Sciences, Semel Institute for Neuroscience and Human Behavior, UCLA, Los Angeles, CA, USA; [3]Harbor-UCLA Medical Center and Los Angeles BioMedical Research Institute, Department of Pediatrics, Torrance, CA, USA; [4]Miller Children's Hospital, Long Beach, CA, USA; [5]LAC+USC Medical Center, Department of Pediatrics, Los Angeles, CA, USA; [6]UCLA Brain Injury Research Center, Dept of Neurosurgery and Division of Pediatric Neurology, Mattel Children's Hospital, Los Angeles, CA, USA; [7]Department of Psychology, UCLA, Los Angeles, CA, USA; [8]Brain Research Institute, UCLA, Los Angeles, CA, USA; [9]Departments of Neurology, Pediatrics, Psychiatry, Radiology, Engineering, and Ophthalmology, USC

**Abstract**

Traumatic brain injury (TBI) can disrupt the white matter (WM) integrity in the brain, leading to functional and cognitive disruptions that may persist for years. There is considerable heterogeneity within the patient group, which complicates group analyses. Here we present improvements to a tract identification workflow, automated multi-atlas tract extraction (autoMATE), evaluating the effects of improved registration. Use of study-specific template improved group classification accuracy over the standard workflow. The addition of a multi-modal registration that includes information from diffusion weighted imaging (DWI), $T_1$-weighted, and Fluid-Attenuated Inversion Recovery (FLAIR) further improved classification accuracy. We also examined whether particular tracts contribute more to group classification than others. Parts of the corpus callosum contributed most, and there were unexpected asymmetries between bilateral tracts.

## 1 Introduction

Traumatic brain injury (TBI) is the leading cause of death and disability in children and adolescents. TBI can cause extensive white matter (WM) damage, which can still be detectable years post-injury. Diffusion weighted imaging (DWI) is useful in studying WM disruptions caused by brain injury, offering a non-invasive means to assess possible diffuse axonal injury (DAI). DAI is frequently associated with poor outcome, but can only be definitively diagnosed *post mortem* [1]. The structural damage

and considerable heterogeneity within the TBI patient population can complicate brain imaging studies, especially inter-subject registration. Here we evaluated improvements in a DWI analytical workflow, automated multi-atlas tract extraction (autoMATE). We use study specific templates, and register images using information from three modalities (DWI, T1, and FLAIR) instead of one.

Fluid-Attenuated Inversion Recovery (FLAIR) is often collected in TBI research due to its sensitivity to lesions. The long inversion time ($T_1$) of FLAIR suppresses the signal from CSF leading to improved differentiation of lesions relative to some $T_2$-weighted sequences [2]. DWI has been applied in TBI research fairly recently, offering better anatomical resolution than conventional CT for detecting and localizing ischemia, DAI, and other TBI-associated neuropathologies [3, 4]. $T_1$-weighted imaging provides a high-resolution anatomical scan that offers a standard target for registration. By combining information from all three modalities, we hoped to leverage the benefits of each, resulting in a more accurate registration.

AutoMATE has been used to analyze WM integrity following TBI, and performs well even in injured tissue [5, 6]. Here we sought to improve the workflow further. We tested the initial workflow and compared it with an intermediate workflow with one alteration, and the final process with two alterations on the same dataset of 31 moderate-to-severe TBI (msTBI) patients and well-matched healthy controls.

# 2 Methods

## 2.1 Subjects and Image Acquisition

TBI participants were recruited from 4 Pediatric Intensive Care Units (PICUs) at Level 1 Trauma Centers in Los Angeles County. Healthy controls, matched for age, sex, and educational level, were recruited from the community through flyers, magazines, and school postings. Participants were studied in the post-acute phase (2-6 months post-injury). We included 31 TBI participants (7 female, 14.3 average age) and 40 controls. *Inclusion criteria*: non-penetrating moderate-severe TBI (intake or post-resuscitation Glasgow Coma Scale (GCS) score between 3 and 12, or higher GCS with positive imaging findings), 8-18 years old at injury, right handed, normal vision, English proficiency. *Exclusion criteria*: history of neurological illness or injury, motor deficits or metal implant preventing safe MRI scanning, history of psychosis, ADHD, Tourette's, learning disability, mental retardation, or autism.

Participants were scanned with 3T MRI (Siemens Trio) with whole-brain anatomical and 66-gradient diffusion imaging. Diffusion-weighted images (DWI) were acquired with the following acquisition parameters: GRAPPA mode; acceleration factor PE=2; TR/TE=9500/87 ms; FOV=256x256mm; isotropic voxel size=2 mm. 72 images were collected per subject: 8 $b_0$ and 64 diffusion-weighted images ($b$=1000 s/mm$^2$).

## 2.2 Tractography

AutoMATE (automated multi-atlas tract extraction) is described fully in prior papers [7-9]. Briefly, autoMATE labels tracts of interest from the whole brain tractography based on template atlases. While many tract labeling tools use only a single template, the strength of autoMATE is that it uses 5 templates, increasing the robustness and generalizability of results. Raw DWI images were visually checked for

artifacts, resulting in 2 participants being excluded from all analyses due to extensive slice dropout (not included in above participant count). DWI images were corrected for eddy-current induced distortions using the FSL tool "eddy_correct" (http://fsl.fmrib.ox.ac.uk/fsl/). DWI scans were skull-stripped using FSL tool "BET" (default parameters). Eddy correct deformations were applied to the gradient vectors. Fractional anisotropy (FA) measures the degree to which water is diffusing preferentially in one direction (along axons). MD (mean diffusivity) is a measure of the average diffusivity across all 3 primary eigenvectors. RD (radial diffusivity) is the average of the eigenvalues corresponding to the 2 non-primary eigenvectors, and AD (axial diffusivity) is the eigenvalue corresponding to the primary eigenvector. FA, MD, RD, and AD maps were computed using FSL tool "dtifit". Whole-brain DWI tractography was performed with Camino (http://cmic.cs.ucl.ac.uk/camino/). The maximum fiber turning angle was set to 35°/voxel to limit biologically implausible results, and tracing stopped when FA dropped below 0.2, a threshold that is somewhat standard in the field.

### 2.3 Fiber Clustering and Label Fusion

The standard autoMATE templates are 5 WM tract atlases constructed from healthy 20-30 year olds, as detailed previously [7-9]. These templates will be referred to as the **standard template**. For this project, we also constructed 5 new WM atlases from 5 adolescents in the study (2F/3M, 14-18 years old, all healthy controls). These templates will be referred to as the **study specific template**. The atlas used to identify tracts in the templates was based on the "Eve" brain atlas [10], and includes 19 major WM tracts: the bilateral corticospinal tract, bilateral cingulum, bilateral inferior fronto-occipital fasciculus, bilateral inferior longitudinal fasciculus, bilateral uncinate, bilateral parahippocampal cingulum, left arcuate fasciculus (the right arcuate is too asymmetric for population studies to be practical [11]), and corpus callosal tracts divided into 6 segments – frontal, precentral gyrus, postcentral gyrus, parietal, temporal, and occipital. The Eve atlas was registered, linearly and then non-linearly, to each subject's FA map using ANTs (Advanced Normalization Tools [12]) and its ROIs were correspondingly warped to extract 18 tracts of interest for each subject based on a look-up table [10]. ROI registration was visually checked for all subjects, and all passed quality control. While registration is difficult in injured brains, the registration tools in the ANTs library have been shown to work well [13].

**Basic registration**: Each subject's FA map was further registered non-linearly using ANTs SyN to each of the 5 *standard templates*. **Intermediate registration**: Each subject's FA map was further registered non-linearly to each of the 5 *study specific templates*. **Multi-modal registration**: Each subject's averaged $b_0$, FLAIR, and $T_1$-weighted image ($T_1$w) were registered linearly then non-linearly to each of the 5 *study specific template*'s $b_0$, FLAIR, and $T_1$w images respectively. Since each modality provides an improved resolution and is sensitive to different aspects of brain structure, they are expected to contribute different information during the registration process. First, each subject's FLAIR and $T_1$w images were linearly registered to their averaged $b_0$ image using the FSL tool "flirt" bringing all three modalities to a common space. ANTs SyN was then used to perform a multi-channel registration to simultaneously warp three images from each subject to the corresponding template images. The $T_1$w images were registered using a cross-correlation coefficient (CC)

similarity metric and was also weighted the highest as it provided the best resolution, followed by FLAIR images registered using mutual information (MI) and weighted 2nd highest, and lastly the $b_0$ images were registered using MI and weighted the least. The transformations were then applied to each subject's FA map, resulting in finely registered FA images to each of the 5 *study specific templates*. This is shown in **Figure 1**. All registrations were visually inspected for quality, and all passed quality control. At this point there are 3 separate processing streams. For each processing stream, the 18 tracts from each atlas were then warped to the subject space based on the deformation field from the above-referenced registration steps [14]. We refined fiber

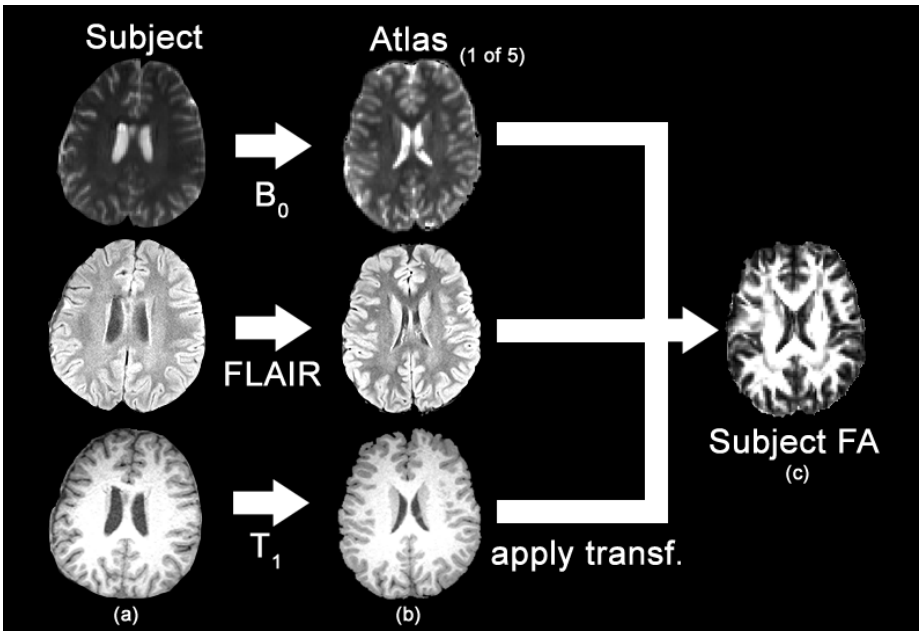


**Figure 1. (a)** Each subject's $b_0$, FLAIR, and $T_1$-weighted image are first linearly then non-linearly registered to its respective atlas image. **(b)** This step is repeated for each of the five atlases. **(c)** The resulting transformations are then applied to each subject's FA image, resulting in an FA image finely registered to each of the five atlas FAs.

extractions of each tract based on the distance between the warped corresponding tract of each atlas and the subject's fiber candidates from ROI extraction. Individual results from the 5 atlases were fused. We visually inspected the resulting fiber bundles. For each of the 18 WM tracts, we selected one example subject to display group analysis results (this step was consistent across processing streams). We extracted FA, MD, RD, and AD along the tracts at this point, output as 8155x15 matrices, with each point in the matrix corresponding to tract coordinates.

### 2.4 Support Vector Machine

Support vector machines (SVMs) [15] are one popular form of supervised learning model that we used to classify our connectivity features, to differentiate connectivity patterns in TBI and normal development. Clearly other machine learning models are possible, but here we chose SVMs as their properties are well understood. SVMs

classify 2-class data by training a model, or classification function, to find the optimal hyperplane between the 2 classes in the data. Let $x_i \in \mathbb{R}^d$ represent the connectivity feature vectors, where $d$ is the dimension of the feature set of interest and $Y_i = \pm 1$ be their label with -1 and 1 representing TBI and control. Our target hyperplane is:

$$\langle w,x\rangle + b = 0,$$

where $w \in \mathbb{R}^d$ should separate as many data points as possible. We find this hyperplane by solving the L2-norm problem:

$$\arg\min_{w,b,v} \left(\frac{1}{2}\langle w, w\rangle + D\sum_i v_i^2\right),$$

such that

$$y_i(\langle w,x_i\rangle + b) \geq 1 - v_i, \qquad v_i \geq 0$$

where $v_i$ are slack variables and $D$ is a penalty parameter. In many instances, a hyperplane cannot be found that completely separates the 2 classes of data, and slack variables are added to create soft margins to separate most of the points.

Our classification design was to test the information provided by the point-wise WM integrity estimates with repeated stratified 10-fold cross-validation [16]. We repeated the cross-validation 10 times. Each repeat represents a different random grouping of dataset for 10-fold cross-validation. For cross-validation (CV), our performance metrics were balanced accuracy (average of sensitivity and specificity), accuracy (number of correctly identified subjects divided by the total number of subjects), sensitivity (true positives [TP] divided by total positives), specificity (true negatives [TN] divided by total negatives), and F1 (2 * ((precision * sensitivity) / (precision + sensitivity)), where precision is TP divided by total positive calls). We used the linear SVM implementation in scikit-learn 0.16.1 (http://scikit-learn.org/) with the default parameters. The input for the SVM was the point-wise estimates of FA, MD, RD, and AD across all tract indices, input as 8155x15 matrices for each subject.

## 3 Results

We calculated the average displacement across all subjects, across all 5 template atlases, across the whole brain, for each of the 3 registrations tested. For the single channel registration with the standard templates, the average displacement magnitude across all subjects was 3.0%. For the single-channel registration with the study specific templates, the average displacement magnitude across all subjects was 3.1%. For the multi-channel registration with the study specific templates, the average displacement magnitude across all subjects was 3.7%. As another check of registration, we extracted the volume of the thalamus in native space and compared it to the volumes extracted after each transformation. This was done across 10 healthy controls. The average difference in thalamic volume between native space and each of our 3 registrations was: basic – 4.2%, intermediate – 2.3%, multi-modal – 3.1%. The average difference in thalamic volume between each registration step was: basic vs. intermediate – 2.1%, intermediate vs. multi-modal – 5.6%.

### 3.1 Study specific template – intermediate registration

The creation of a study specific template was the first improvement to the workflow. The standard autoMATE templates are taken from 20-30 year old healthy controls, while the study specific templates include 5 14-18 year olds (2F/3M, all healthy controls). Use of a more age-appropriate template, taken from the sample, improved nearly all measures of group discrimination across FA, MD, and RD. SVM based on AD gave mixed results. The classification outputs can be seen in **Table 1**. T-tests of the 10 CV repeats showed these improvements were largely significant.

### 3.2 Multi-modal registration

The second improvement to the workflow involved the inclusion of multiple image modalities for the template registration, as well as the same study specific templates used in the intermediate registration. This step brought further improvement to the classification outputs for all measures. These results can be seen in **Table 1**. T-tests of the 10 CV repeats showed the improvements over single channel were only significant for one measure (indicated in **bold** in the table), but over the original registration they were highly significant (indicated in *italics* in the table).

| | **Single channel registration / Standard template** | | | | |
|---|---|---|---|---|---|
| | *BAC* | *Accuracy* | *Sensitivity* | *Specificity* | *F1* |
| **FA** | 0.7995 | 0.8039 | 0.8640 | 0.7350 | 0.8222 |
| **MD** | 0.7621 | 0.7692 | 0.8525 | 0.6717 | 0.7992 |
| **RD** | 0.7823 | 0.7892 | 0.8670 | 0.6975 | 0.8143 |
| **AD** | 0.7475 | 0.7580 | 0.8525 | 0.6425 | 0.7920 |
| | **Single channel registration / Study specific template** | | | | |
| | *BAC* | *Accuracy* | *Sensitivity* | *Specificity* | *F1* |
| **FA** | 0.8012 | 0.8118 | 0.8850 | 0.7175 | 0.8414 |
| **MD** | **0.8004** | **0.8043** | **0.8350** | **0.7658** | **0.8228** |
| **RD** | **0.8042** | **0.8132** | 0.8775 | **0.7308** | **0.8405** |
| **AD** | 0.7325 | 0.7520 | **0.8775** | **0.5875** | 0.7978 |
| | **Multi-modal registration / Study specific template** | | | | |
| | *BAC* | *Accuracy* | *Sensitivity* | *Specificity* | *F1* |
| **FA** | 0.8038 | 0.8146 | *0.8900* | 0.7175 | *0.8437* |
| **MD** | ***0.8104*** | *0.8143* | 0.8450 | *0.7758* | *0.8328* |
| **RD** | *0.8029* | *0.8134* | *0.8875* | *0.7183* | *0.8432* |
| **AD** | 0.7379 | 0.7751 | *0.8850* | *0.5908* | *0.8031* |

**Table 1.** Comparison of SVM outputs from the basic, intermediate, and multi-modal registration protocols. **Bolded** entries are significantly improved over the previous step, *italicized* entries for the multi-modal step are significantly improved over the initial step, as shown in *t*-tests of the 10 CV repeats.

### 3.3 Most robust tracts

The analysis to this point was completed using all tract data, but we were interested to see whether specific tracts aided in classification more than others. We ran a separate classification examining each tract alone. For this, we ran SVM as above, but with data from each tract separately input into the SVM. The balanced accuracy across all 19 tracts is depicted in **Figure 2**, averaged across the tract. We

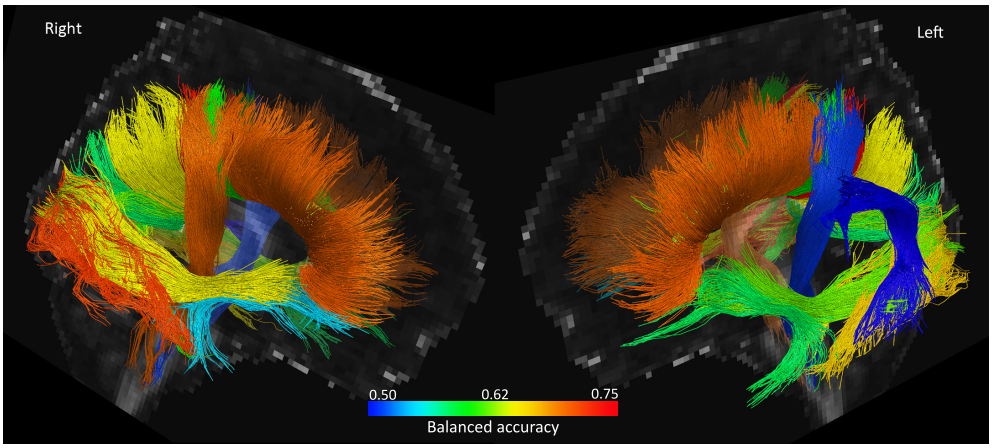


**Figure 2.** Balanced accuracy (BAC) across the 19 tracts computed from MD along tract. Colors correspond to BAC, according to the legend.

computed this on FA, MD, RD, and AD, but we display results here only for RD. The CC frontal, CC postcentral, and right inferior longitudinal fasciculus (ILF) had the highest BAC. There appeared to be an asymmetry as well, with right hemisphere tracts having higher average BAC than left hemisphere tracts (0.664 vs. 0.615).

## 4 Discussion

TBI can cause widespread damage to the brain, but the pattern of injury can differ based on severity, location, type, and any number of unknown premorbid patient characteristics. This heterogeneity can complicate inter-subject registration, which is critical for accurate and generalizable results. Here we aimed to improve this step, by including templates generated from subjects in the study, and by using a multi-modal registration.

Using study-specific templates improved the classification accuracy from resulting tract-wise WM integrity measures. This is an expected outcome, as templates matched for age and scan protocol should be more similar to the patient images to be registered. The images we selected for the multi-modal registration were chosen for their particular sensitivity to detecting pathology caused by brain injury. Conventional MRI ($T_1$w) identifies lesions more accurately than computed tomography (CT) does. DWI can indicate possible DAI, ischemia, and demyelination post-injury. FLAIR, one of the sequences most commonly used by neuroradiologists for clinical purposes, can detect contusions, edema, and subarachnoid and intraventricular hemorrhage [17]. Other researchers have used multi-modal approaches for segmentation and registration [18-20]. Creating study-specific templates and choosing disease-specific sequences tailors this workflow to the study of TBI and improves our ability to study its effects on the brain.

We also examined how tracts differed in their individual contributions to the classification, finding considerable variation in classification accuracy across the tracts. The tracts with the highest balanced accuracy were the CC frontal segment, CC postcentral gyrus, and right ILF. The corpus callosum is one of the most well-

documented areas of disruption following a brain injury, so it is not surprising that callosal segments had high BAC [21]. Of our 31 TBI patients, 3 had large space occupying lesions on the left hemisphere 1 had a large lesion on the right hemisphere, 10 had small lesions on either the right or left hemisphere, and the remainder had no visible lesions. These large left hemisphere lesions likely increased the within-group variance, affecting the accuracy classification based on information from left hemisphere tracts.

## 5 Conclusion

We present step-wise changes to the DWI processing workflow, including use of study-specific templates and incorporating information from multiple modalities when registering images. Each step improved on the previous method in our ability to accurately classify subjects, ending with accuracy around 0.81 for FA, MD, and RD. Additionally, we show that certain tracts aid more in this classification than others, with the CC frontal segment, CC postcentral gyrus segment, and right ILF emerging as providing the most discriminative information. This improved workflow will aid us in further multi-modal investigations of recovery following pediatric TBI.

**Acknowledgements:** This study was supported by the NICHDS (R01 HD061504). ELD is supported by a grant from the NINDS (K99 NS096116). ELD, FR, JV, GP, JF and PT are also supported by NIH grants to PT: U54 EB020403, R01 EB008432, R01 AG040060, and R01 NS080655. CCG is supported by the UCLA BIRC, NS027544, NS05489, Child Neurology Foundation, and the Jonathan Drown Foundation. Scanning was supported by the Staglin IMHRO Center for Cognitive Neuroscience. We gratefully acknowledge the contributions of Alma Martinez and Alma Ramirez in assisting with recruitment and study coordination. Finally, the authors thank the participants and their families for contributing their time.

## References

1. Parizel, P., Özsarlak, Ö., Van Goethem, J., Van Den Hauwe, L., Dillen, C., Verlooy, J., Cosyns, P. and De Schepper, A. (1998). Imaging findings in diffuse axonal injury after closed head trauma. European Radiology 8, 960-965.
2. Ashikaga, R., Araki, Y. and Ishida, O. (1997). MRI of head injury using FLAIR. Neuroradiology 39, 239-242.
3. Ashwal, S., Holshouser, B.A. and Tong, K.A. (2006). Use of Advanced Neuroimaging Techniques in the Evaluation of Pediatric Traumatic Brain Injury. Developmental Neuroscience 28, 309-326.
4. Xu, J., Rasmussen, I.-A., Lagopoulos, J. and Håberg, A. (2007). Diffuse axonal injury in severe traumatic brain injury visualized using high-resolution diffusion tensor imaging. Journal of neurotrauma 24, 753-765.
5. Dennis, E.L., Jin, Y., Villalon-Reina, J., Zhan, L., Kernan, C., Babikian, T., Mink, R., Babbitt, C., Johnson, J. and Giza, C.C. (2015). White matter disruption in moderate/severe pediatric traumatic brain injury: advanced tract-based analyses. NeuroImage: Clinical 7, 493-505.
6. Dennis, E.L., Ellis, M.U., Marion, S.D., Jin, Y., Moran, L., Olsen, A., Kernan, C., Babikian, T., Mink, R., Babbitt, C., Johnson, J., Giza, C.C., Thompson, P.M. and

Asarnow, R.F. (2015). Callosal function in pediatric traumatic brain injury linked to disrupted white matter integrity. Journal of Neuroscience 35, 10202-10211.
7. Jin, Y., Shi, Y., Zhan, L., de Zubicaray, G.I., McMahon, K.L., Martin, N.G., Wright, M.J. and Thompson, P.M. (2013). Labeling white matter tracts in HARDI by fusing multiple tract atlases with applications to genetics. In: *10th Proc IEEE Int Symp Biomed Imaging*: San Francisco, CA, pps. 512-515.
8. Jin, Y., Shi, Y., Zhan, L., Gutman, B., de Zubicaray, G.I., McMahon, K.L., Wright, M.J., Toga, A.W. and Thompson, P.M. (2014). Automatic clustering of white matter fibers in brain diffusion MRI with an application to genetics. NeuroImage.
9. Jin, Y., Shi, Y., Zhan, L., Li, J., De Zubicaray, G.I., McMahon, K.L., Martin, N.G., Wright, M.J. and Thompson, P.M. (2012). Automatic Population HARDI White Matter Tract Clustering by Label Fusion of Multiple Tract Atlases. Medical image computing and computer-assisted intervention : MICCAI ... International Conference on Medical Image Computing and Computer-Assisted Intervention 7509, 147-156.
10. Zhang, Y., Zhang, J., Oishi, K., Faria, A.V., Jiang, H., Li, X., Akhter, K., Rosa-Neto, P., Pike, G.B., Evans, A., Toga, A.W., Woods, R., Mazziotta, J.C., Miller, M.I., van Zijl, P.C.M. and Mori, S. (2010). Atlas-guided tract reconstruction for automated and comprehensive examination of the white matter anatomy. NeuroImage 52, 1289-1301.
11. Catani, M., Allin, M.P., Husain, M., Pugliese, L., Mesulam, M.M., Murray, R.M. and Jones, D.K. (2007). Symmetries in human brain language pathways correlate with verbal recall. PNAS 104, 17163-17168.
12. Avants, B.B., Tustison, N.J., Song, G., Cook, P.A., Klein, A. and Gee, J.C. (2011). A reproducible evaluation of ANTs similarity metric performance in brain image registration. NeuroImage 54, 2033-2044.
13. Kim, J., Avants, B., Patel, S., Whyte, J., Coslett, B.H., Pluta, J., Detre, J.A. and Gee, J.C. (2008). Structural consequences of diffuse traumatic brain injury: a large deformation tensor-based morphometry study. NeuroImage 39, 1014-1026.
14. Jin, Y., Shi, Y., Jahanshad, N., Aganj, I., Sapiro, G., Toga, A.W. and Thompson, P.M. (2011). 3D elastic registration improves HARDI-derived fiber alignment and automated tract clustering. In: *8th Proc IEEE Int Symp Biomed Imaging*. IEEE: Chicago, IL, pps. 822-826.
15. Cortes, C. and Vapnik, V. (1995). Support-vector networks. Machine Learning 20, 273-297.
16. Kohavi, R. (1995). A study of cross-validation and bootstrap for accuracy estimation and model selection. In: *IJCAI*, pps. 1137-1145.
17. Weiss, N., Galanaud, D., Carpentier, A., Naccache, L. and Puybasset, L. (2007). Clinical review: prognostic value of magnetic resonance imaging in acute brain injury and coma. Crit Care 11, 230.
18. Irimia, A., Wang, B., Aylward, S.R., Prastawa, M.W., Pace, D.F., Gerig, G., Hovda, D.A., Kikinis, R., Vespa, P.M. and Van Horn, J.D. (2012). Neuroimaging of structural pathology and connectomics in traumatic brain injury: Toward personalized outcome prediction. Neuroimage Clin 1, 1-17.
19. Wang, B., Prastawa, M., Irimia, A., Chambers, M.C., Sadeghi, N., Vespa, P.M., Van Horn, J.D. and Gerig, G. (2013). Analyzing imaging biomarkers for traumatic

brain injury using 4D modeling of longitudinal MRI. In: *2013 IEEE 10th International Symposium on Biomedical Imaging*. IEEE, pps. 1392-1395.
20. Wang, B., Liu, W., Prastawa, M., Irimia, A., Vespa, P.M., van Horn, J.D., Fletcher, P.T. and Gerig, G. (2014). 4d Active Cut: An Interactive Tool for Pathological Anatomy Modeling. Proceedings / IEEE International Symposium on Biomedical Imaging: from nano to macro. IEEE International Symposium on Biomedical Imaging 2014, 529-532.
21. Hulkower, M.B., Poliak, D.B., Rosenbaum, S.B., Zimmerman, M.E. and Lipton, M.L. (2013). A Decade of DTI in Traumatic Brain Injury: 10 Years and 100 Articles Later. American Journal of Neuroradiology 34, 2064-2074.